

# Towards Efficient and Accurate Detection of On-Chip Fail-Slow Failures for Many-Core Accelerators

Junchi Wu  
Peking University  
Beijing, China  
2501111908@stu.pku.edu.cn

Xinfei Wan  
Peking University  
Beijing, China  
2300013096@stu.pku.edu.cn

Zhuoran Li  
Peking University  
Beijing, China  
2200012710@stu.pku.edu.cn

Yuyang Jin  
Tsinghua University  
Beijing, China  
jyy17@mails.tsinghua.edu.cn

Guangyu Sun  
Peking University  
Beijing, China  
gsun@pku.edu.cn

Yun Liang  
Peking University  
Beijing, China  
ericlyun@pku.edu.cn

Diyu Zhou  
Peking University  
Beijing, China  
diyu.zhou@pku.edu.cn

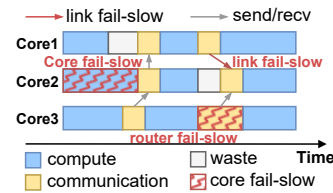
Youwei Zhuo  
Peking University  
Beijing, China  
youwei@pku.edu.cn

**Abstract**—Many-core accelerators are essential for high-performance deep learning, but their performance is undermined by widespread fail-slow failures. Detecting such failures on-chip is challenging, as prior methods from distributed systems are unsuitable due to strict memory limits and their inability to track failures across the hardware topology.

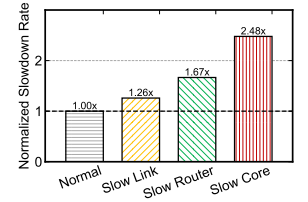
This paper introduces SLOTH, a lightweight, hardware-aware framework for practical on-chip fail-slow detection in many-core accelerators. SLOTH combines workload-aware instrumentation for operator-level monitoring with minimal overhead, on-the-fly trace compression to operate within kilobytes of memory, and a novel topology-aware ranking algorithm to pinpoint a failure’s root cause. We evaluate SLOTH on a wide range of representative DNN workloads. The results demonstrate that SLOTH reduces the storage overhead by an average of  $115.9\times$ , while achieving an average fail-slow detection accuracy of  $86.77\%$  and a false positive rate (FPR) of  $12.11\%$ . More importantly, SLOTH scales effectively across different many-core accelerator architectures, making it practical for large-scale deployments.

## I. INTRODUCTION

Many-core accelerators, integrating tens to thousands of processing cores on a single chip or via multi-chiplet packaging, have emerged as the backbone of modern applications. To support massive parallelism, these architectures rely on a tightly coupled design, where cores are interconnected via a high-bandwidth Network-on-Chip (NoC) to enable frequent, low-latency communication. This fabric allows them to efficiently handle throughput-demanding workloads [13], [14], [78], [80], [83], ranging from large-scale model training and inference to graph analytics [11], [17], [64] and scientific simulations [2], [50], [69]. As a result, many-core accelerators are increasingly deployed across diverse platforms from edge



(a) Fail-slow failures on different hardware components.



(b) Normalized execution time of ResNet-50.

Fig. 1: Fail-slow failure and its impact on overall performance of DNN inference. Execution times are measured on a  $4\times 4$  core accelerator with a  $10\times$  performance degradation fail-slow of different components.

devices to data centers, delivering significant gains in performance and energy efficiency compared to traditional multi-core CPUs and GPGPUs [35], [44], [73], [74].

However, the scale and complexity of these accelerators introduce a critical reliability challenge: **the fail-slow failure** [23]. Unlike fail-stop failures that cause system crashes [3], [56] or incorrect outputs [10], a fail-slow component remains functionally correct but operates at a significantly reduced speed. The causes of these failures are widespread across the whole system (Figure 1a), ranging from physical aging and wear [1], [5], [24], [72] to dynamic resource contention [6], [77] and thermal stress. For instance, performance degradation triggered by high temperatures in DRAM can reach 24% to 52% [42], [61]. The system-level impact of such local slowdowns is severe, particularly in tightly synchronized workloads where progress is dictated by the slowest task—the straggler

TABLE I: Comparison of hardware failure detection approaches in different scenes.

Target Scenario	Detection Approach	Failure Pattern	Failure Model	Validation Method	Memory Overhead
Cloud System	Sieve [15]	Fail-Slow	Latency	Simulation	8 GiB
	Groot [71]	Fail-Stop Fail-Slow	Error Degradation	Real Plat.	20 GiB
Micro Service	Sleuth [21]	Fail-Slow	Contention	Simulation Real Plat.	84 MiB
	Sage [20]	Fail-Slow	Latency Contention	Real Plat.	Not Mentioned
Distributed System	IASO [55]	Fail-Slow	Timeout	Real Plat.	1.6 MiB Per Hour
	Perseus [46]	Fail-Slow	Latency	Real Plat.	Not Mentioned
Many-Core Accelerator	ADR [45]	Fail-Slow	Packet Loss Latency	Real Plat.	Not Mentioned
	SLOTH (Ours)	Fail-Slow	Degradation	Simulation	150 KiB

effect. Our simulations quantify this cascading impact: as shown in Figure 1b, a single fail-slow event in a link, router, or core increases total execution time by  $1.26\times$ ,  $1.67\times$ , and  $2.48\times$ , respectively. This degradation is exacerbated by **propagation**: due to tight connectivity, hardware backpressure from a slow core rapidly spreads to healthy upstream neighbors. [41], [46], [47], [76]. Furthermore, these failures are often **transient**, appearing only under specific bursty workloads or thermal conditions, which makes them difficult to reproduce or detect once the system state changes.

The characteristics of fail-slow failures, especially the transiency, mandate an **on-chip** detection paradigm, as traditional off-chip mechanisms are fundamentally ill-suited to capture such phenomena. On the one hand, **the transient nature of these failures creates a critical detection gap for external observers**. Off-chip monitoring typically relies on periodic polling or remote telemetry, operating at a coarse granularity and with significant transmission latency. By the time the status data reaches an external host, the micro-architectural stall effectively vanishes, rendering the external detector blind to the fleeting root cause. On the other hand, **precise diagnosis requires high-resolution traffic data, which inevitably collides with the I/O bandwidth wall**. Streaming continuous, fine-grained execution traces off-chip imposes a prohibitive bandwidth overhead. This heavy data movement not only effectively saturates limited I/O resources but also induces a parasitic effect: the diagnosis traffic competes with the actual workload for memory access, distorting the very system behavior it attempts to measure. Therefore, effective identification necessitates a shift to on-chip detection. Crucially, to accommodate hardware constraints, this approach must be lightweight and capable of performing in-situ statistical aggregation, capturing the failure root cause locally without the latency or bandwidth penalties of external analysis.

While fail-slow detection has been explored in microservices and distributed systems (Table I), adapting these paradigms to many-core accelerators is impeded by two

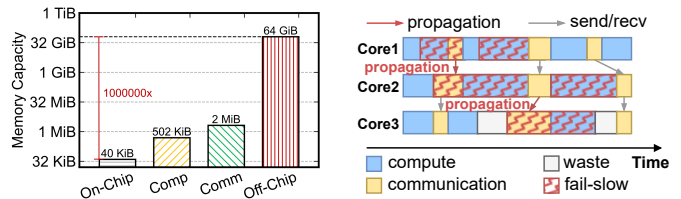


Fig. 2: Challenges for detecting fail-slow failures: (a) On-chip, off-chip memory capacity versus computation and communication tracing log size for tracing DarkNet-19 for 1 second on a  $4\times 4$  core processor. (b) Slowdown propagates across cores along communication dependencies.

challenges. First, **many-core systems have strict on-chip memory limits**. Standard runtime tracing strategies [46], [55] and graph-based analyses [21], [33], [71] rely on capturing extensive execution logs, incurring massive storage overheads (e.g., Gigabytes for Sieve and Groot) that contradict the hardware reality shown in Figure 2a. Even a minimal 1-second trace of DarkNet-19 necessitates 2 MiB just for communication logs; this creates an unbridgeable gap with on-chip SRAM capacity (typically 64 KiB per core), rendering continuous in-situ tracing spatially infeasible. Second, **existing methods are lack of hardware topological awareness**. While graph-based methods analyze software dependencies, they struggle to distinguish root causes from propagated symptoms due to the complex on-chip interconnect topology. As illustrated in Figure 2b, a fail-slow failure in Core 1 triggers a cascading slowdown: the delayed data transmission propagates along the communication links, forcing downstream cores (Core 2 and Core 3) into involuntary wait states. Because existing methods focus on application-level stragglers without accounting for the underlying hardware backpressure dynamics, they inevitably conflate the symptoms with the cause, misidentifying the backpressured victims as the culprits.

Therefore, an effective detection mechanism for many-core accelerator must be both **lightweight** to be efficient and **hardware-aware** to be accurate. A lightweight design must operate within tight memory limits, while a hardware-aware approach must analyze the accelerator’s hardware topology to localize the root cause.

In this paper, we present **SLOTH**<sup>1</sup> (Slowdown Localization via **O**n-chip **T**racing and **H**ierarchical graph analysis), a fail-slow detection framework with a comprehensive workflow that spans data collection, compression, storage, and analysis to meet these requirements.

First, we propose a workload-aware probe mechanism that enables lightweight performance data tracing without interfering with program execution. It automatically analyzes the computation graph to identify insertion points, collecting operator-level performance metrics. We further design a sketch-based data structure to compress and store the collected traces efficiently. To narrow down the failure candidates, we employ

<sup>1</sup>The source code of SLOTH along with failure datasets and traces are available at <https://anonymous.4open.science/r/sloth-91D7>

a group-based fail-core detection in combination with under-determined linear system-based fail-link inference. To capture both software and hardware propagation of fail-slow failures, we reconstruct the communication dependency graph onto the hardware topology, and incorporate temporal information through hierarchical extension. Finally, we introduce FailRank, an iterative ranking algorithm that computes a fail-slow score for each component, thereby identifying the most likely root cause of fail-slow failures. In summary, our contributions are:

- **SL-Compiler:** A workload-aware probe mechanism that leverages compiler-based instrumentation to automatically insert probe at operator boundaries. This enables operator-level tracing with minimal overhead while capturing fine-grained metrics.
- **SL-Recorder:** A compact, on-the-fly, sketch-based data structure that filters and compresses trace data. This design preserves critical failure signatures while operating within the strict memory constraints of on-chip SRAM.
- **SL-Tracer:** A topology-aware, multi-stage diagnosis pipeline that integrates the software communication graph with the hardware topology. It uses a novel algorithm—FailRank—to accurately trace failure propagation across cores and links, and pinpoint the true root cause.

We evaluate SLOTH on a many-core accelerator simulator using representative DNN workloads with injected fail-slow failures. Experimental results show that, on average, SLOTH reduces the storage overhead of detection traces by  $115.9\times$ , achieves 86.77% fail-slow detection accuracy with 12.11% FPR, and scales effectively to larger core counts.

## II. BACKGROUND

### A. Many-Core DNN Accelerators

Many-core DNN accelerators integrate numerous cores into a scalable on-chip network to exploit massive parallelism for deep learning workloads. Figure 3 illustrates the fundamental components of such an architecture. Inter-core communication is enabled by the Network-on-Chip (NoC), which can adopt various topologies. Common structures include 2D-mesh, torus, and ring networks [18], [83], while more complex topologies such as hypercube and dragonfly have also been proposed [19]. These topologies can support different communication patterns and, in specific scenarios, provide higher bandwidth. In this work, we focus on mesh-based networks, as they are implementation-friendly and are the most widely adopted topology in practice [22], [68]. Each core is directly connected to a router and consists of three major components: a control unit, a compute unit, and a scratchpad memory. The control unit manages intra-core resource allocation and task scheduling. The compute unit executes DNN operators and typically integrates specialized accelerators such as vector units or tensor units optimized for matrix operations. The scratchpad memory is a small, high-speed SRAM placed adjacent to the compute unit, typically less than 64 KiB in capacity, storing activations, weights, and intermediate results.

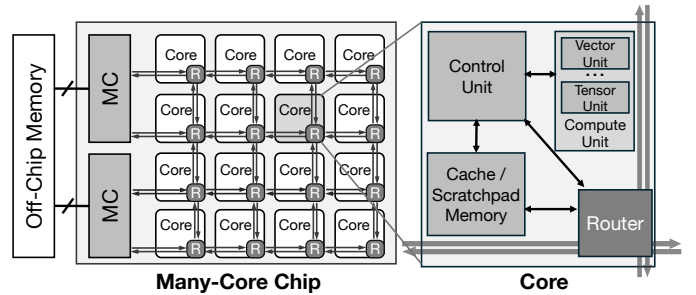


Fig. 3: Overview of a many-core DNN accelerator with 2D-mesh network and its intra-tile organization.

It is explicitly managed by software or compilers, thereby simplifying hardware coherence logic [4], [16].

Based on the hardware organization above, many-core DNN accelerators employ a dataflow execution model to maximize concurrency and overlap computation with communication [7], [9], [28]. In this paradigm, DNN models are represented as computation graphs, where nodes denote operators (e.g., convolution, pooling) and edges represent data dependencies between layers [12], [54]. Execution is data-driven—an operator is triggered as soon as its input features and weights become available, avoiding the cost of global synchronization. DNN operators are mapped onto cores according to data locality and the layer-wise computational workflow, while the scheduler within each core monitors operator readiness, fetches operands from local or neighboring cores, and dispatches them to compute units. Intermediate features are routed through the NoC according to the communication pattern derived from the DNN computation graph. This fine-grained pipelining of data movement and operator processing improves hardware utilization, but also creates tight coupling between cores: delays in one core’s execution can propagate through dependent operators across the chip, amplifying the performance impact of fail-slow failures in DNN inference.

### B. Hardware Failures

In many-core DNN accelerators, hardware components are subject to a wide range of failures that invariably degrade inference performance. Based on their behavioral characteristics, common hardware failures are classified into two categories: fail-slow and fail-stop [23], [55].

For cores, bit flips can alter register values, leading to incorrect computation results or even program crashes [27], [60], which are characteristic of fail-stop failures. In contrast, performance variations caused by internal resource contention, workload imbalance, or hardware aging typically degrade overall performance [67], [85], and are categorized as fail-slow failures. For memory, permanent physical defects as well as software bugs or mismanagement can trigger system crashes, thus are fail-stop failures. Meanwhile, memory leaks or buffer overflows could consume significant system resources, causing response delays and performance degradation, which belong to fail-slow failures [47], [79]. For NoC, transient bandwidth reductions on links or low router port utilization can decrease

overall throughput and prolong program execution time [8], [70], both of which are fail-slow failures. In contrast, routing-induced deadlocks can completely stall communication, making them fail-stop failures [66].

In this paper, we focus on detecting fail-slow failures caused by core-level performance variance and link-level bandwidth degradation—both of which are prevalent and, more importantly, can propagate along communication and execution dependencies, leading to system slowdowns.

### III. THE SLOTH FRAMEWORK

SLOTH is an automated framework for detecting and locating fail-slow failures in many-core DNN accelerators. As shown in Figure 4, the framework is composed of three main components. **SL-Compiler** instruments DNN operators with lightweight probes at operator boundaries, collecting fine-grained runtime execution traces with minimal overhead. **SL-Recorder** then filters irrelevant traces and compresses redundant ones, producing a compact yet representative list of communication and execution patterns. Finally, **SL-Tracer** leverages the compressed data to construct multi-level communication graphs and performs the FailRank algorithm on them, pinpointing fail-slow cores or links responsible for performance degradation. Together, these components form a systematic pipeline that bridges low-overhead monitoring with high-accuracy failure diagnosis.

#### A. Input and Output

As shown in the left of Figure 4, the inputs to SLOTH consist of: (1) **DNN Workload**: DNN models are composed of operators such as convolution, pooling, and data movement instructions including *read*, *send*, and *recv*. The framework supports arbitrary operator-to-core mappings [25], [36], [84]. In our implementation, we use a Gemini-like [7] mapping strategy for evaluation; (2) **Arch Config**: the specification of the target many-core DNN accelerator architecture, which enables analysis across different hardware platforms; (3) **Probe Config**: parameters that determine what execution information to collect, where to place probes at operator boundaries, and how to store the collected trace data; (4) **Failure Model**: definitions of fail-slow behavior, including failure duration, performance degradation rate, and affected components.

The outputs fall into two categories: **fail-slow detection results**, including the root causes, SL-Recorder’s optimal compression parameters, and the overhead of data collection and storage; and **system-level metrics**, such as total inference time and per-layer execution latency.

#### B. SL-Compiler

Traditional tracing approaches face a trade-off between coverage and overhead: exhaustive collection is prohibitively expensive, while reactive collection risks missing critical failure signatures. To address this challenge, we propose SL-Compiler, a DNN-aware probe instrumentation tool that analyzes the hierarchical structure and explicit data dependencies of DNN workloads to insert eBPF (extended Berkeley Packet

TABLE II: Components of probe’s five-tuple definition.

Component	Option	Description
Fragment	Exec	Record calculation related traces
	Route	Record communication traces
	Mem	Record memory access traces
Type	Comp	Match compute instructions
	Comm	Match communication instructions
	IO	Match input / output instructions
Location	Pre	Before the target instruction
	Post	After the target instruction
	Surround	Before & after the instruction
Level	Inst	Aggregate trace at instruction level
	Stage	Aggregate trace at stage level
Structure	List	Store traces in list manner
	Sketch	Store traces using SL-Recorder

Filter) inspired probes, reducing monitoring overhead while preserving the ability to capture fail-slow behaviors.

**Probe Abstraction.** SL-Compiler decomposes the monitoring process into three configurable abstractions, as summarized in Table 1. Probe fragments define what data to collect—whether computation time (Exec), communication latency (Route), or memory access (Mem). Insertion tracepoints specify where to place probes by combining an instruction type filter (Type: Comp, Comm, or IO) with a relative position (Location: Pre, Post, or Surround). Data maps determine how to organize collected traces, supporting both fine-grained (Level: Inst) and coarse-grained (Level: Stage) aggregation, with flexible storage structures (Structure: List for dense access or Sketch for memory efficiency). Together, these abstractions enable users to express complex monitoring strategies through a compact five-tuple configuration.

**DNN-graph-guided Insertion.** A key innovation of SL-Compiler is its ability to automatically generate probe configurations by analyzing the DNN computation graph and its mapping to the target architecture. As illustrated in Figure 5, this process takes as input the workload mapping—which specifies how DNN operators are distributed across cores—and performs static analysis to identify critical monitoring points. The process proceeds in three steps. First, it parses the computation graph to extract the layer sequence, data dependencies, and operator types (e.g., Conv2D, Pooling). Second, it analyzes the workload-to-core mapping to determine which cores execute communication-intensive operations (requiring Route probes) versus computation-heavy operators (requiring Exec probes). For instance, in Figure 5b, it identifies that Conv layers dominate computation and automatically inserts post-execution probes ([Exec, Comp, Post, Stage, List]) to capture their execution time. Similarly, in Figure 5c, it detects inter-core data transfers and inserts pre-communication probes to monitor link latency. Third, it generates the instrumented code by inserting lightweight probe fragments at the identified tracepoints. Importantly, this process is fully automated, freeing users from manual instrumentation while still supporting custom probe specifications for specialized analysis needs.

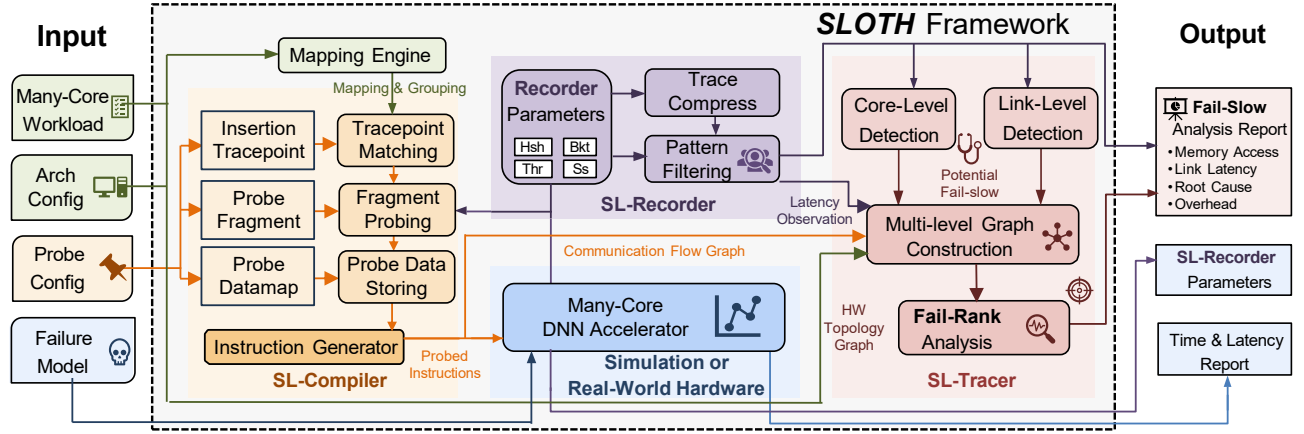


Fig. 4: Overview of SLOTH.

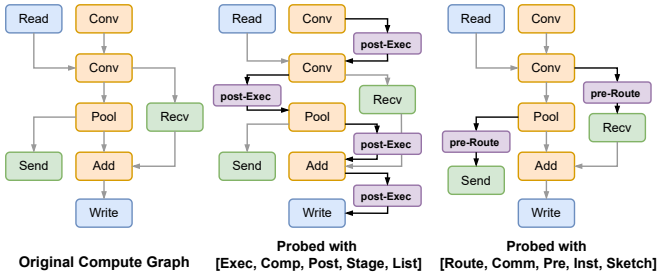


Fig. 5: Examples of SL-Compiler probing.

**Operator-level Semantic Collection.** Beyond basic performance metrics, SL-Compiler captures high-level DNN operator semantics to facilitate root cause analysis. Each probe records not only the standard execution attributes—such as start/end timestamps, and core ID, but also DNN-specific metadata that characterizes the computational context. For computation probes, this includes the operator type (e.g., Conv2D, GEMM), input/output tensor dimensions, and floating-point operation count (FLOPs). For communication probes, it records the data volume transferred, the source and destination cores, and the corresponding tensor being communicated. This semantic information serves two critical purposes: (1) it enables layer-aware analysis in SL-Tracer, allowing the framework to correlate slowdowns with specific DNN layers; and (2) it facilitates communication pattern recognition, helping distinguish between normal inter-layer data transfers and anomalous traffic caused by fail-slow failures. For example, if a Conv layer exhibits unexpectedly high communication latency, the recorded tensor dimensions can reveal whether the slowdown stems from excessive feature map sizes or from degraded link bandwidth.

### C. SL-Recorder

To reduce the storage overhead, we propose SL-Recorder, a lightweight on-the-fly data structure for trace compression and pattern-based filtering. The data structure is also called Fail-Slow Sketch as it is inspired by sketches. As illustrated in Figure 6, Fail-Slow Sketch operates in two stages. In Stage-

### Algorithm 1: Fail-Slow Sketch Insertion

**Input:** instruction trace  $e$ ; number of hash tables  $d$ ; number of buckets  $m$ ; pattern threshold  $H$

```

1 for each  $i \in [1, d]$  do
2    $Index \leftarrow Hash(e.key) \bmod m$ ;
3    $bucket \leftarrow HashTable[i][Index]$ ;
4   if  $bucket.key$  equals to  $e.key$  then
5     increase the frequency of  $e$  by 1;
6     if frequency of  $e \geq H$  then Insert_Stage_2( $e$ ,
7       attributes);
8   else if  $bucket$  is empty then
9      $bucket.key \leftarrow e.key$ ;
10    set the frequency of  $e$  to 1;
11  else
12    decrease the frequency of  $e$  by 1;
13    if frequency of  $e$  is 0 then clear  $bucket$  to empty;

13 Function Insert_Stage_2( $e$ ,  $attr$ )
14 if  $e.key \notin Stage-2$  then
15   if  $Stage-2.length \geq MAX\_LENGTH$  then evict the earliest
16   pattern in Stage-2;
17   insert  $e$  into Stage-2;
18   return 1;
19 else
20   Update( $e.key$ ,  $attr$ );
  
```

1, a Running Track identifies frequently occurring traces with similar execution behaviors. In Stage-2, the common patterns of the traces are extracted to reduce storage redundancy.

**Stage-1** consists of  $d$  bucket arrays, each associated with a distinct hash function. These hash functions map trace features that characterize execution patterns to bucket indices. Each array contains  $m$  buckets, and each bucket has two fields: trace pattern (key) and its frequency. When the frequency exceeds a threshold  $H$ , the corresponding trace pattern is considered as a potential candidate for fail-slow pattern.

**Stage-2** maintains a list of candidate fail-slow patterns and their associated attributes. This list supports operations such as updates and evictions, and its maximum length ( $MAX\_LENGTH$ ) is determined based on the characteristics of the workload. In this stage, traces with the same pattern are

compressed, and statistical summaries are computed to support root cause analysis. When the list reaches its maximum capacity, the Fail-Slow Sketch evict the most “healthy” pattern to make room for newly observed patterns.

**Insertion.** Given an input trace  $t$ , Fail-Slow Sketch first extracts its pattern features and computes the target bucket index using corresponding hash function. The trace is then inserted into the bucket (donated as  $b$ ). As shown in Algorithm 1, there are three possible cases:

*Case 1:*  $t$  is not in the bucket, and  $b$  is currently empty. In this case, the trace pattern is stored in  $b$ , the frequency is set to 1, and the insertion completes.

*Case 2:*  $t$  is not in the bucket, and  $b$  is occupied. In this case, the frequency of  $b$  is decremented by 1. If the frequency drops to zero, the bucket is cleared, and the algorithm terminates.

*Case 3:*  $t$  is in the bucket  $b$ . In this case, the frequency counter is incremented by 1. If the frequency reaches the threshold  $H$ , the trace pattern is considered a candidate for Stage-2. If the pattern already exists in the Stage-2 list, its statistics are updated via update function; otherwise, a new pattern entry will be created. If the Stage-2 list has reached its capacity, typical replacement strategies such as frequency-based, probability-based, or arrival-time-based policies can be applied. In our design, we use an arrival-time-based replacement policy to ensure correct insertion of trace patterns.

**Update.** Given a trace pattern and its attributes, the update operation modifies the corresponding entry in the Stage-2 pattern list to maintain the overall statistical information. For communication patterns, this includes updating metrics like data volume. For computation patterns, the update includes floating-point operation count, core id, and other relevant metrics. Additionally, all trace patterns have to maintain the timestamp of their first appearance and their duration, which are essential for root cause analysis.

**Example:** Figure 6 shows a running example of Fail-Slow Sketch. To insert coming trace *Comp4*, Stage-1 extracts its pattern *cp4*. *cp4* has been inserted into corresponding bucket before, so Fail-Slow Sketch adds the frequency of the bucket

by 1 and finishes inserting. When inserting trace *Comm2*, the frequency of the bucket reaches threshold  $H = 10$  and there is space in Stage-2’s pattern list. Therefore, Fail-Slow Sketch create a new trace pattern (*cm2,10,128,5*) for *Comm2* through *Creation* operation, in which *cm2* is the trace pattern, 10 is *cm2*’s frequency, 128 is the data volume and 5 is the destination of communication. Besides, Fail-Slow Sketch performs *Update* operation for existing pattern *cm1* and *Eviction* operation for deleted pattern *cp3*. After inserting all the traces, the compressed traces, also the trace patterns are stored in Stage-2’s pattern list.

**Mathematical Analysis.** It can be proved that increasing the number of hash functions  $d$  can effectively improve the retention probability, but also increases computational overhead; increasing the number of buckets  $m$  helps reduce hash collisions, but also increases storage overhead. We provide a proof for the conclusion as follow.

Given a fixed workload, let  $N$  be the number of instruction traces,  $f_i$  be the frequency of trace  $t_i$ ,  $B_j[k]$  be  $k$ -th bucket of  $j$ -th bucket array, and  $F_{i,j,k}$  be the number of traces mapped to bucket  $B_j[k]$  except for trace  $t_i$ .

LEMMA 3.1. For any trace pattern  $R_i$  in the instruction traces, let  $P(R_i)$  be its retention probability in Stage-2, then

$$P(R_i) \geq 1 - \left(\frac{N - f_i}{m(f_i - H)}\right)^d$$

PROOF. For a single bucket  $A_j[k]$  in Stage-1 which records trace  $t_i$ , according to the insertion algorithm, we have

$$f_i - F_{i,j,k} \leq A_j[k].freq \leq f_i$$

Since the hash function is uniformly distributed, the probability of mapping to a specific bucket is  $\frac{1}{m}$ , so the expectation of  $F_{i,j,k}$  is

$$E[F_{i,j,k}] = \sum_{t \neq t_i} f_t \frac{1}{m} = \frac{N - f_i}{m}$$

For a trace pattern  $R_i$  in Stage-2 and threshold  $H$ , there must be a  $j \in \{1, 2, \dots, d\}$  such that

$$f_i - F_{i,j,k} \geq H \Leftrightarrow F_{i,j,k} \leq f_i - H$$

By Markov inequality, we can evaluate the probability of not recoding trace pattern  $R_i$  with one hash function

$$P(F_{i,j,k} \geq f_i - H) \leq \frac{E[F_{i,j,k}]}{f_i - H} = \frac{N - f_i}{m(f_i - H)}$$

Since we have  $d$  hash functions, so the retention probability of a trace pattern  $R_i$  is

$$P(R_i) \geq 1 - \left(\frac{N - f_i}{m(f_i - H)}\right)^d$$

We further conduct parameter sensitivity analysis (Section IV-D) and design space exploration (Section IV-E) to determine the optimal configuration of SL-Recorder.

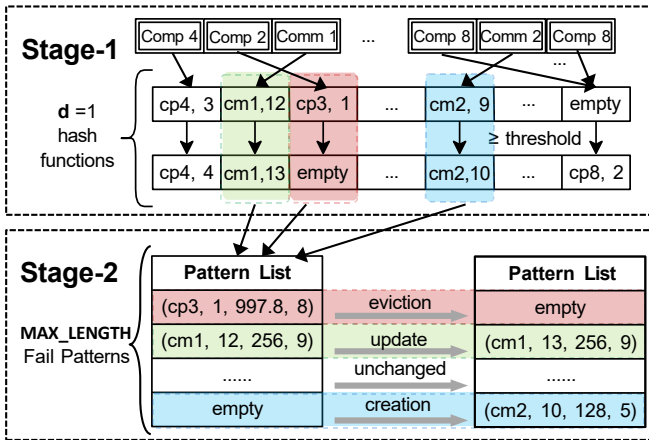


Fig. 6: An example of Fail-Slow Sketch ( $d=1$ ).

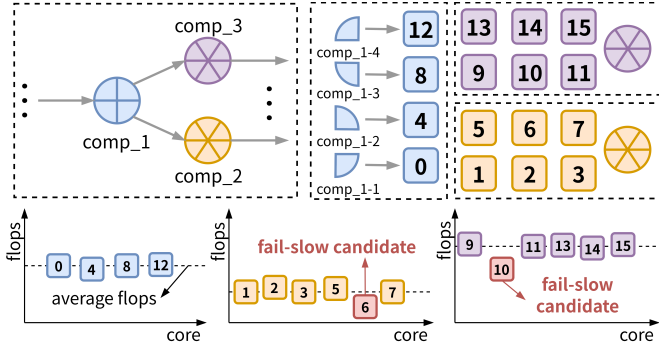


Fig. 7: Core level fail-slow detection.

#### D. SL-Tracer

SL-Tracer is designed to identify and localize the root cause fail-slow failures. It follows a detection–construction–analysis pipeline. First, core-level detection and link-level detection are performed to identify potential fail-slow candidates. These candidates, together with workload’s communication dependency graph and the hardware topology, are integrated together to construct multi-level communication graph (MCG). Finally, the FailRank algorithm operates on this graph to quantify the likelihood of each candidate being the root cause, providing a ranked explanation of fail-slow components.

1) *Core-Level Fail-Slow Detection*: The goal of core-level fail-slow detection is to identify candidate fail-slow cores. Our method performs the detection in a stage-aware manner, leveraging the mapping from DNN to many-core accelerator.

As illustrated in Figure 7, we first partition computation instructions by execution stage (e.g., network layers), ensuring that only tasks with comparable semantics are grouped together. Next, cores are clustered according to the workload-to-core mapping. Each group therefore contains volume-equivalent computations executed across different cores, making their performance directly comparable.

Within each group, we measure the performance of each core in terms of floating-point operations (FLOPs) per unit time. The group average serves as the baseline, and we perform outlier detection to highlight cores whose FLOPs are significantly lower than the baseline. These outliers are flagged as fail-slow candidates. For example, in Figure 7, core 6 and 10 deviate from their peers and are thus marked as candidates. Each candidate is further assigned a fail-slow probability, derived from its performance variance distribution. This probability is then used as the initial fail-slow score for the FailRank algorithm (Sec III-D3).

2) *Link-Level Fail-Slow Detection*: The goal of link-level fail-slow detection is to identify candidate fail-slow interconnect links. Since such fail-slow behaviors cannot be directly observed under limited hardware visibility, we infer them from communication traces collected by SL-Recorder. Specifically, we formulate the problem as a statistical inference task, where observed end-to-end communication delays are decomposed to estimate the bandwidth of individual links.

For each communication event, we record four key attributes: the transferred data volume, the measured transmission time, and the index of the source and destination cores. Leveraging the deterministic routing algorithm of the 2D-mesh interconnect, we map each event to the set of links traversed along its multi-hop path, thereby associating observed end-to-end latency with individual link bandwidths.

To estimate link bandwidth, we transform the problem into a set of linear equations by turning each link’s bandwidth  $b_i$  into its inverse  $\theta_i = \frac{1}{b_i}$ . Each communication event yields an equation of the form  $Ax^T = T_{comm}$ , where  $A$  represents the link composition of paths,  $x$  represents  $\theta_i$  vector and  $T_{comm}$  represents the observed transmission times.

Because the system is underdetermined and affected by measurement noise, we adopt the Expectation–Maximization (EM) algorithm to infer link bandwidths. EM algorithm iteratively estimates link bandwidths by alternating between (1) computing expected path-level delays given current bandwidth estimates and (2) updating bandwidth estimates to maximize the likelihood of the observed traces. This process converges to a set of link bandwidths that best explain the data, even under partial or noisy observations.

To assess the likelihood of fail-slow behavior, we calculate the fail-slow probability using the bandwidth gamma distribution model. These probabilities are then assigned as the initial fail-slow scores of links in the FailRank algorithm.

3) *Fail-Slow Root Cause Analysis*: To localize fail-slow root causes, we construct MCG that integrates hardware topology, execution dependencies, and runtime tracing data. This augmented graph captures how performance degradation propagates across cores and links, turning the localization into a graph-based inference problem. On this foundation, we design **FailRank**, a PageRank-inspired algorithm that quantifies the propagation probability of fail-slows, enabling accurate root cause identification.

**MCG Definition.** MCG is defined as a layered graph  $G = (V, E)$  that integrates task dependency and hardware topology, shown in the right of Figure 8. Each node  $v \in V$  represents a core in a time window, bounded with a set of computation instructions. The likelihood for being root cause of node  $v$  is quantified by a fail-slow score  $s(v) \in [0, 1]$  (determined

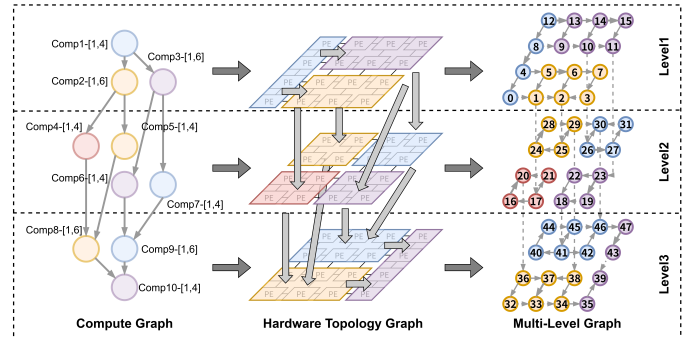


Fig. 8: Construction of multi-level communication graph.

in Sec III-D1). Each directed edge  $e = (u, v) \in E$  denotes communication dependency between two cores, bounded with a set of communication instructions. The edge is associated with a propagation weight  $w(u, v)$ , capturing the probability that performance degradation propagates from core  $u$  to  $v$ .

To construct the MCG, we perform a depth-first search (DFS) on the workload’s computation graph  $G_c = (V_c, E_c)$ . As illustrated in Figure 8,  $G_c$  is a directed acyclic graph (DAG). For each dependency edge  $(x, y) \in E_c$ , we first determine the physical cores  $p(x)$  and  $p(y)$  assigned to tasks  $x$  and  $y$ . The mapping  $p : V_c \rightarrow E_h$  links computation nodes to hardware cores in the hardware topology  $G_h = (V_h, E_h)$ . The communication path between  $p(x)$  and  $p(y)$  is then identified as a sequence of hardware links  $\{e_1, e_2, \dots, e_k\} \in E_h$ . For each traversed link  $e_i$ , we increment its traffic volume  $T(e_i)$  by the transported data size of  $(x, y)$ .

After traversing the entire DAG, we normalize the traffic volumes to derive edge propagation weights. Specifically, for each core  $u \in V_h$ , let  $Out(u) = \{(u, v) \in E_h\}$  denote its outgoing links. This normalization ensures that  $\sum_{(u, v') \in Out(u)} w(u, v') = 1$ , making  $w(u, v)$  interpretable as the probability of failure propagation through link  $(u, v)$ . The resulting MCG thus provides a structured, probabilistic view of how fail-slow behaviors may spread across both computation and communication dependency within a level.

To capture cross-level interactions, we introduce virtual DRAM nodes that connect levels. These nodes represent interactions through memory, such as fetches or writes between different levels. Edges connected to a DRAM node represent inter-level dependencies, showing how fail-slow may propagate across levels. This vertical connection adds a temporal dimension to MCG, allowing the FailRank algorithm to analyze the timing and causality of fail-slows.

**FailRank Algorithm.** To localize fail-slow root causes from core-level and link-level candidates, we propose FailRank, a graph-based iteration algorithm inspired by PageRank, which identifies fail-slow root causes on MCG. Unlike PageRank that only updates node scores based on their neighbors with uniform transition probabilities, FailRank incorporates propagation weights of their neighbor links.

The algorithm initialize fail-slow scores with the probabilities obtained in core-level and link-level detection, denoted as  $s_0(v)$  for node  $v$  and  $l_0(u, v)$  for edge  $(u, v)$ . At each iteration, a node’s score is updated not only from its neighboring nodes but also from the weighted contributions of connecting links:

$$s^{(k+1)}(v) = (1 - \lambda)s_0(v) + \lambda \sum_{(u, v) \in E} w(u, v) s^{(k)}(u)$$

where  $w(u, v)$  is the normalized propagation weight of edge  $(u, v)$  defined in Sec III-D3. Each link’s score is updated by three factors: the propagation weight, the fail-slow scores of its endpoint node  $u$ , and its current score:

$$l^{(k+1)}(u, v) = \alpha w(u, v) + \beta s^{(k)}(u) + \gamma l^{(k)}(u, v)$$

where  $\alpha, \beta, \gamma$  are workload-dependent coefficients. Users can flexibly tune the edge update weights according to workload

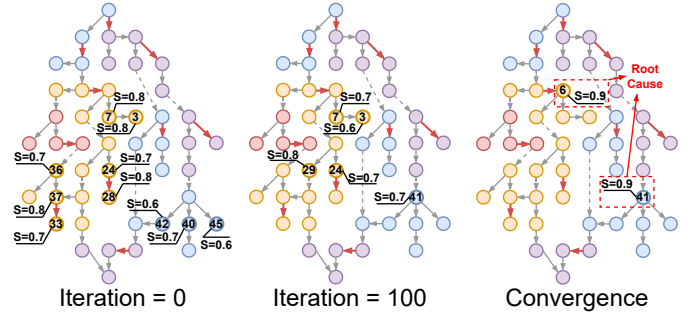


Fig. 9: An example of FailRank algorithm.

characteristics—for instance, setting a higher  $\alpha$  for applications with intensive communication request. In our experiments, we set  $\alpha = 0.1, \beta = 0.3, \gamma = 0.6$ .

As Figure 9 shows, FailRank starts with initial fail-slow candidates and iteratively updates their scores until convergence. Each node is assigned a fail-slow score  $s$ , as annotated in the figure (e.g.,  $s = 0.8, 0.7$ ), which reflects the likelihood of being the root cause. Edges indicate communications between cores. Red edge has higher communication volume, while the dashed edge shows memory-access dependencies between levels. During iterations, the nodes with higher fail-slow scores and edges with heavier traffic exert stronger influence on their neighbors. After convergence, FailRank normalizes node and edge scores within each level of the MCG using a softmax function, yielding a probability distribution that pinpoints the most likely fail-slow root cause.

## IV. EVALUATION

### A. Experimental Setup

**Evaluation Platform.** We implement an event-driven simulator for many-core DNN accelerators using SimPy [52], a Python-based discrete-event simulation framework. The simulator can capture concurrent execution across thousands of processes, accurately modeling resource contention and inter-core communication. To ensure the reliability of our simulator, we validated it against the Dataflow Abstract Machine (DAM) framework [82], a parallel simulator for dataflow systems. We cross-verified total execution cycles produced by our simulator with DAM’s Communicating Sequential Processes with Time (CSPT) model on several dataflow graphs under identical workload configurations.

To faithfully capture real-world hardware behavior, our simulator incorporates statistical models [29], [59] for key performance parameters based on established distributions observed in production systems [32], [49]. For computing capacity, we model the computing capacity  $P_{core}$  of each core as a normally distributed random variable:  $P_{core} \sim N(\mu_c, \sigma_c^2)$  where  $\mu_c$  represents the expected processing capacity and  $\sigma_c^2$  quantifies the runtime variability. For link bandwidth, we model the transmission time  $T_{link}$  using a Gamma distribution:  $T_{link} \sim Gamma(\alpha, \beta)$  to capture latency variation caused by bandwidth. The shape parameter controls the asymmetry of latency distribution, while the rate parameter reflects the average link throughput.

TABLE III: Fail-slow detection accuracy.

Algorithm	DarkNet-19		GoogLeNet		VGG		ResNet-50		Binary Tree	
	Acc.↑(%)	FPR↓(%)								
Thres	50.92(138/271)	53.29(81/152)	51.65(141/273)	54.61(83/152)	45.45(125/275)	59.09(91/154)	51.29(139/271)	56.77(88/155)	60.44(165/273)	46.05(70/152)
Mscope	68.20(193/283)	33.97(53/156)	67.14(188/280)	37.58(59/157)	68.46(191/279)	35.26(55/156)	64.47(176/273)	45.22(71/157)	79.20(217/274)	23.75(38/160)
IASO	31.65(163/515)	58.58(215/367)	37.14(156/420)	43.28(116/268)	22.53(164/728)	73.93(433/585)	13.54(221/1632)	89.85(1347/1499)	38.27(175/457)	52.20(166/318)
Perseus	66.38(235/354)	32.44(73/225)	80.75(235/291)	6.17(10/162)	45.37(235/518)	60.93(237/389)	16.84(235/1395)	87.99(1144/1266)	78.33(235/300)	11.11(19/171)
ADR	10.58(235/2222)	92.73(1941/2093)	11.17(235/2102)	92.29(1821/1973)	11.06(235/2123)	92.37(1842/1994)	11.17(235/2102)	92.29(1821/1973)	11.30(235/2079)	92.20(1798/1950)
SLOTH (Ours)	80.40(242/301)	12.64(22/174)	88.30(264/299)	13.64(24/176)	87.38(263/301)	14.61(26/178)	82.79(255/308)	16.48(30/182)	94.98(265/279)	3.18(5/157)

**Workloads.** We evaluate SLOTH on four representative DNN models that exhibit diverse characteristics: GoogLeNet [65], DarkNet-19 [57], VGG [63], and ResNet-50 [26]. These workloads span a range of architectural patterns from highly parallel branching structures to memory-intensive linear pipelines. The input dimensions of all workloads are configured to match typical throughput-oriented inference (batch size = 64). For controlled microbenchmark analysis, we additionally construct a binary tree computation graph where each node performs matrix operations. This synthetic workload isolates communication patterns from complex DNN semantics, facilitating ablation studies on probe latency and storage overhead.

The mapping configurations are generated by the Gemini framework [7], which specifies the tensor partitioning strategy and the block-to-core assignment. This deterministic mapping allows us to inject fail-slow failures at specific cores and observe their propagation through the computation graph.

**Fail-Slow Dataset.** We construct a fail-slow dataset comprising 152 failure instances characterized by three parameters: failure location (core-level or link-level at a 7:3 ratio), duration (uniformly distributed between 0–10 s), and slowdown rate (fixed at 10×). Failures are reused across workloads if they affect execution; those occurring on unused resources are excluded. For larger architectures (4×4, 6×6, 8×8), we generate additional failures proportional to the expanded resource count. To ensure balanced evaluation, we construct an equal number of negative samples by modifying DNN structures to produce workload traces without fail-slow failures. This dataset enables comprehensive evaluation of detection accuracy, localization precision, and robustness across diverse failure scenarios, workloads, and system scales.

**Baseline.** We compare SLOTH against five baseline methods originally designed for microservices, distributed storage, or server clusters. We adapt these methods to the many-core DNN accelerator domain with in-house implementations, and all the methods share the same raw trace collection infrastructure for fair comparison. For methods providing risk-level outputs, we classify moderate risk or higher as fail-slow. The parameters used by each method have been searched to match our data. Detailed description of baselines is as follows:

(1) **Threshold Filtering (Thres)** monitors raw performance metrics (per-core computation time, link latency) and flags components exceeding 2× the nominal latency threshold derived from workload profiling as fail-slow.

(2) **Microscope (Mscope)** [40] constructs a directed acyclic graph of inter-service dependencies and ranks root causes using random walk-based scoring. We model data dependencies

between operators as service dependencies.

(3) **IASO** [55]. A peer-based detection framework that converts timeout signals into scores using AIMD combined with DBSCAN clustering. We treat each core as a peer node, using execution time violations as timeout signals.

(4) **Perseus** [46] builds polynomial regression models on latency-versus-throughput distributions, employing PCA and DBSCAN for outlier detection. We construct core-level model and use the 99.9th percentile as the detection threshold.

(5) **Adaptive Detection at Runtime (ADR)** [45] monitors both value and update frequency of performance variables using sliding windows with adaptive thresholds based on historical percentiles.

## B. Fail-slow Root Cause Detection

We evaluate detection effectiveness across five workloads. As shown in Table III, baseline methods exhibit distinct limitations that impact their accuracy.

Thres and Mscope can detect both node and link fail-slows but suffer from low sensitivity. Thres misses 40-50% of true fail-slows across workloads, as static thresholds cannot adapt to dynamic performance variations. Mscope achieves slightly better recall but still misses 20-32% of cases, and its FPR reaches 33-54% due to incorrect attribution in complex dependency graphs. IASO, Perseus, and ADR detect more true fail-slows but are limited to node-level detection. More critically, these methods misclassify propagated slowdowns as root causes, resulting in high FPR. ADR’s adaptive thresholding suffers from the highest FPR (91-93%) by treating persistent propagated effects as independent failures, while Perseus shows workload-dependent behavior: it achieves low FPR (6.17%) on structurally simple GoogLeNet but degrades significantly on complex models like ResNet-50 (FPR: 87.99%).

Workload characteristics significantly influence detection difficulty. Binary Tree’s simple structure and regular communication patterns yield the highest accuracy across all methods. Conversely, DarkNet-19’s uniform workload mapping produces highly correlated traces, degrading inference quality—even SLOTH achieves only 80.4% accuracy here. Complex CNNs (GoogLeNet, VGG, ResNet-50) fall in between, where diverse layers provide richer trace information but also introduce more propagation paths that confuse baseline methods.

SLOTH outperforms baselines by addressing both node and link fail-slows while explicitly modeling fault propagation through iterative inference. It achieves 80-95% accuracy with low FPR (3-17%), demonstrating robust performance across different workload structures.

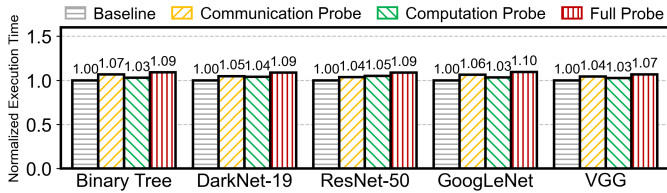


Fig. 10: Time overhead of SL-Compiler probing.

### C. Data Collection Time Overhead

In this experiment, we evaluate the runtime overhead of probe-based data collection under different instrumentation configurations. In the simulator, probe latency is determined by collected data volume—for example, reading the system clock incurs a 10-cycle delay. We use probe-free execution as the baseline and compare three configurations: Communication Probe (instruments communication instructions only), Computation Probe (instruments computation instructions only), and Full Probe (instruments all instructions). Each configuration is repeated multiple times to account for performance variability, with average execution time reported.

Figure 10 shows that probe-based collection introduces minimal overhead. Even under the most extensive instrumentation (Full Probe), execution time increases by at most 10% across all workloads. For targeted scenarios such as Communication Probe—suitable for network performance monitoring—overhead remains below 5%. These results demonstrate that our approach enables fine-grained trace collection with negligible performance impact.

### D. Effectiveness of Storage Overhead Reduction

We evaluate SL-Recorder’s storage efficiency by comparing memory consumption before and after compression. The raw format records full instruction details (index, timestamps, operands, ...) and serves as the baseline. For each workload, we separately measure communication and computation trace sizes, then apply compression to quantify storage savings. We also compare against IASO (communication traces), Perseus and ADR (computation traces)’ memory requirement to demonstrate SL-Recorder’s advantage.

Figure 11 shows that SL-Recorder achieves significant compression compared to both raw traces and IASO. For Binary Tree, raw traces consume 10 MiB and IASO consume 7 MiB, while SL-Recorder compresses to 86 KiB—a 98.8% reduction. Similar results appear across all workloads. IASO’s algorithm

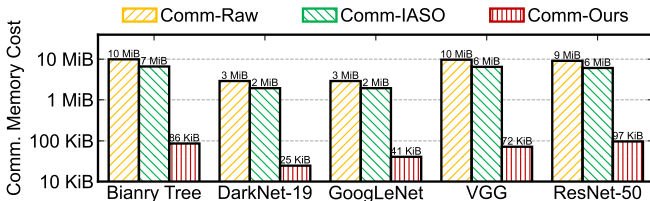


Fig. 11: Memory cost of communication traces with no optimization, IASO and SL-Recorder.

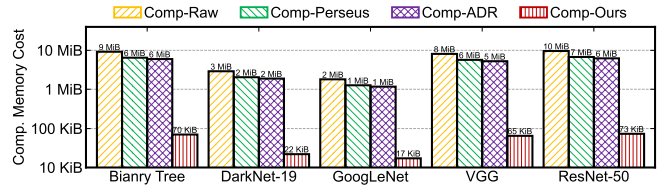


Fig. 12: Memory cost of computation traces with no optimization, Perseus, ADR and SL-Recorder.

only provides marginal savings (30-40% reduction) as it still retains full communication trace. Figure 12 demonstrates similar effectiveness for computation trace. Across all workloads, SL-Recorder consistently achieves 98-99% compression ratios, while Perseus and ADR achieve only 25-50% compression as they retain per-instruction records for regression analysis or adaptive threshold. Overall, SL-Recorder reduces both communication and computation trace storage by over two orders of magnitude across all workloads, significantly outperforming existing approaches and making fine-grained trace collection practical for resource-constrained environments.

Further, we examine how the internal parameters of SL-Recorder influence its compression efficiency. We conduct this experiment on DarkNet-19, varying four parameters: the number of hash functions ( $Hash, H$ ), the number of buckets ( $Bucket, B$ ), the Stage-2 size ( $Size, S$ ), and the pattern-selection threshold ( $Threshold, T$ ). To capture the interaction effects between parameters, we fix two of them at default values and vary the other two, measuring the resulting compression ratio. The results are visualized using heatmaps, where each heatmap illustrates how the compression ratio changes under different parameter combinations.

Figure 13 illustrates the impact of different parameter settings on the compression ratio of SL-Recorder. Among the four parameters,  $H$ ,  $B$ , and  $T$  show a clear influence on compression effectiveness, while  $S$  has little impact. Specifically, a smaller number of hash functions and buckets, as well as a larger threshold, consistently lead to stronger compression. In contrast, varying  $S$  across a wide range does not significantly alter the compression ratio, indicating that this parameter is

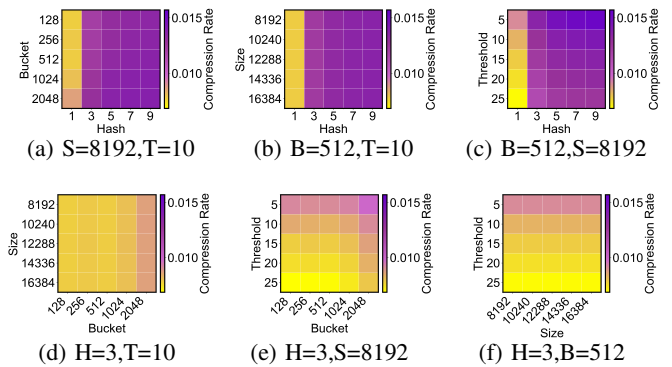


Fig. 13: SL-Recorder compression rate: Impact of the Hash ( $H$ ), Bucket ( $B$ ), Size ( $S$ ), and Threshold ( $T$ ).

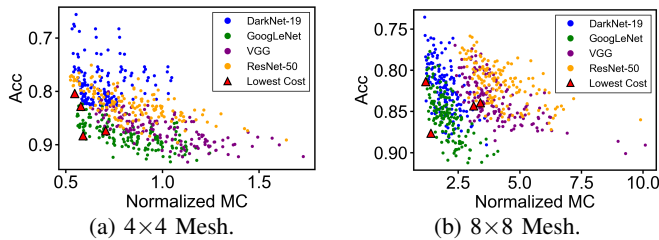


Fig. 14: SL-Recorder Design Space Exploration.

relatively insensitive. These observations suggest that tuning hash, bucket, and threshold values is crucial for achieving high compression efficiency, whereas Stage-2 size can be fixed without noticeably affecting performance.

### E. Design Space Exploration

To find out the optimal configuration of SL-Recorder, we conduct a design space exploration (DSE) across four key parameters: the number of hash functions (*Hash*), the number of buckets (*Bucket*), the Stage-2 size (*Size*), and the pattern-selection threshold (*Threshold*). These parameters jointly determine the compression efficiency and detection accuracy of SLOTH.

We define a composite optimization objective as:  $COST = ACC^\alpha \times R^\beta \times M^\gamma$ , where  $ACC$  represents the detection accuracy,  $R$  denotes the data compression rate, and  $M$  refers to the memory overhead of data structure. By adjusting the hyperparameters  $\alpha, \beta, \gamma$ , users can flexibly prioritize accuracy, compression rate, or memory overhead according to their own deployment requirements. Here we set  $\alpha = -1, \beta = \gamma = 1$ , considering all three objectives equally.

Figure 14a shows the exploration results on a  $4 \times 4$  many-core DNN accelerator, where each point corresponds to a parameter configuration, and different colors represent different workloads. We can observe that the design space exhibits clear trade-offs: configurations with lower memory cost often suffer from degraded accuracy, whereas moderate-cost configurations yield balanced performance. The lowest-cost Pareto-optimal cases are highlighted with red triangles. Figure 14b shows DSE results on a  $8 \times 8$  many-core DNN accelerator, which has the same trade-off like that on  $4 \times 4$  accelerator.

### F. FailRank Convergence Analysis

To demonstrate the efficiency and stability of the proposed FailRank algorithm, we analyze its convergence behavior across various fail-slow scenarios. We quantify the convergence process using the  $L_1$ -norm of the difference between score vectors in consecutive iterations, defined as the error  $\Delta_k = \|\mathbf{v}^{(k)} - \mathbf{v}^{(k-1)}\|_1$ , where  $\mathbf{v}^{(k)}$  denotes the score vector at iteration  $k$ . The iterative process is considered converged when this residual error falls below a strict tolerance threshold, set here to  $\epsilon = 10^{-4}$ .

Figure 15 illustrates the reduction of  $\Delta_k$  over iterations on a logarithmic scale, revealing a distinct and rapid convergence trend. The process typically begins with an initial rapid descent phase during the first few iterations (iterations 1-3), where

the error drops sharply by an order of magnitude as the ranking scores propagate through the immediate neighborhood of the failure. This is immediately followed by a stable decay phase, where the error decreases linearly on the log-scale plot, indicating a geometric rate of convergence as the global ranking stabilizes.

Crucially, the curves representing different fail-slow locations and intensities exhibit highly consistent trajectories, demonstrating that FailRank is robust to variations in failure patterns. In all tested cases, the algorithm satisfies the convergence criterion within approximately 17 iterations. Given that each iteration involves only lightweight matrix-vector operations, this low and bounded iteration count ensures that FailRank incurs negligible runtime overhead, making it well-suited for detection within the resource-constrained environment of many-core accelerators.

### G. Scalability Analysis

To evaluate the scalability of SLOTH, we test its performance on many-core DNN accelerators of different scales. Specifically, we simulate ResNet-50 and DarkNet-19 on  $4 \times 4$ ,  $6 \times 6$ , and  $8 \times 8$  accelerators, and measure the execution time under three probing modes: communication probe, computation probe, and full probe.

The results are shown in Figure 16. For both networks, the overall execution time decreases as the architecture scale grows, which indicates that larger many-core DNN accelerators could provide higher parallelism and better workload distribution. More importantly, the additional overhead introduced by probing remains consistently low across different scales. As illustrated by the red points in the figure, the normalized execution time overhead of the full probe is always below 10%, demonstrating that our framework introduces only marginal overhead even at larger scales.

Figure 17 further evaluates memory efficiency and detection accuracy. As the scale increases, the volume of trace data

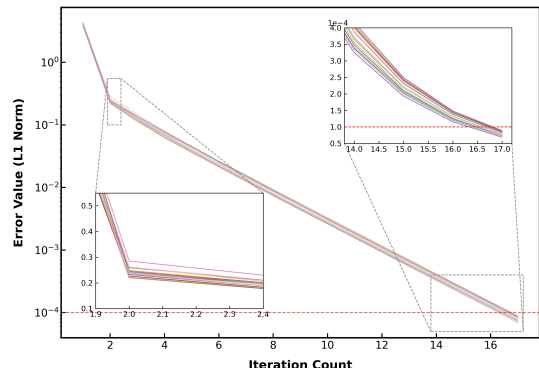


Fig. 15: Convergence analysis of FailRank on different fail-slow cases. The y-axis (log scale) represents the  $L_1$ -norm difference between score vectors of consecutive iterations. The algorithm converges rapidly within 20 iterations for all datasets ( $\epsilon = 10^{-4}$ ).

naturally grows, resulting in higher raw memory cost. However, SL-Recorder consistently achieves nearly  $100\times$  reduction in memory consumption across different scales, showing that the compression ratio is insensitive to architecture scale. Meanwhile, the detection accuracy of fail-slow failures remains stable, with only minor fluctuations and no significant degradation as the architecture grows.

## V. RELATED WORK

**Distributed Tracing.** Existing distributed tracing systems reduce overhead through reactive collection or selective storage [34], [37], [38], [62], but these approaches are often not suitable for diagnosing fail-slow behaviors. For instance, Pivot Tracing [48] enables on-demand instrumentation based on user queries, yet critical early-stage evidence of gradual degradation is often missed. Hindsight [81] uses post-hoc triggers to commit buffered traces, but the performance decay of fail-slow issues may not activate these triggers in time, leading to the loss of crucial data. Similarly, while Sieve [31] applies an attention model to prioritize traces, it is biased towards conspicuous spikes and can overlook the weak, temporally-correlated signals characteristic of a fail-slow. In contrast, our SL-Compiler employs a proactive and structure-aware strategy; by analyzing the DNN’s computational graph to automatically instrument critical dataflows (while also allowing user guidance), it can capture most of the traces indicating fail-slow degradation.

**Trace Storage Optimization.** The sheer volume of trace data needs optimizations for efficient storage [30], [43], [58]. For example, Mint [30] reduces storage footprint by decomposing traces into common patterns and specific attributes. However, this structural compression is agnostic to performance semantics; it does not help in identifying or prioritizing traces that exhibit gradual latency degradation. Other works leverage sketches for data summarization [39], [51], [75]. For example, Dynamic Sketch [75] uses a doorkeeper mechanism to efficiently detect heavy hitters, but it focus on request frequency and is misaligned with fail-slow analysis. Similarly, while SketchLib [53] provides highly optimized sketch implementations for Reconfigurable Match-Action Tables (RMT), its design is incompatible with the stringent on-chip memory constraints. Our SL-Recorder employs a novel two-stage sketch design. By extending traditional sketch features to include latency statistics, it can identify similar workloads

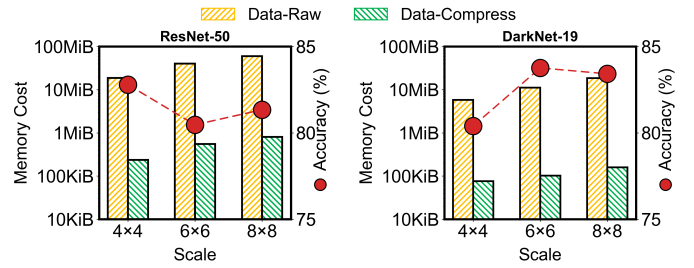


Fig. 17: Scalability of SLOTH: Memory cost and detection accuracy.

within a DNN and dynamically update them to filter the traces that are most indicative of fail-slow behavior.

**Failure Detection and Root Cause Analysis.** Ensuring system reliability requires robust mechanisms for both failure detection and subsequent root cause analysis (RCA) [20], [21], [33], [71]. For instance, ScalAna [33] leverages backtracking on a Program Structure Graph (PSG) to localize root causes. However, its reliance on a purely logical graph, which abstracts away the hardware topology, hinders the diagnosis of communication-related bottlenecks. Another class of methods focuses on component-level metrics [45], [46], [55]. Approaches like IASO [55], using timeout signals and peer-scoring, and ADR [45], which monitors latency and frequency shifts, are effective at identifying node-level slowdowns. Nevertheless, their node-centric perspective fails to capture performance degradation occurring on the communication links themselves. Our SL-Tracer overcomes these limitations using a Multi-level Communication Graph (MCG) that integrates software communication dependencies with the underlying physical topology. By applying an iterative FailRank algorithm on MCG, SL-Tracer can pinpoint the root cause of fail-slow, irrespective of whether the origin is a computational node or a communication link.

## VI. CONCLUSION

In this work, we introduce SLOTH, a tracing and analyzing framework for detecting and localizing fail-slow failures in many-core DNN accelerators. SLOTH provides a full-stack solution that spans lightweight data collection, online trace compression, and graph-based root cause analysis. Specifically, we design SL-Compiler to insert low-overhead tracing probes into DNN workload, SL-Recorder to achieve runtime trace filtering and compression, and SL-Tracer for accurate fail-slow localization. We evaluate SLOTH using a set of representative networks and hardware configurations. Experiments demonstrate the effectiveness of SLOTH. It reduces the storage overhead of detection traces by an average of  $115.9\times$ , while achieving an average fail-slow detection accuracy of 86.77% with an FPR of 12.11%. These results highlight the practicality of SLOTH and its capability to provide scalable fail-slow detection across diverse many-core architectures.

## REFERENCES

- [1] M. Agarwal, B. C. Paul, M. Zhang, and S. Mitra, “Circuit failure prediction and its application to transistor aging,” in *25th IEEE VLSI*

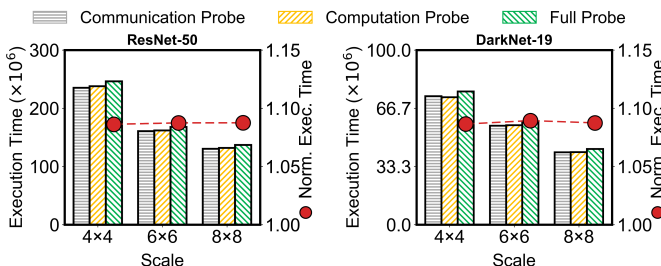


Fig. 16: Scalability of SLOTH: Time overhead.

- Test Symposium (VTS'07)*, IEEE. Berkeley, CA, USA: IEEE, 2007, pp. 277–286.
- [2] A. Ahmadzadeh and H. Sarbazi-Azad, “Fast and scalable quantum computing simulation on multi-core and many-core platforms,” *Quantum Information Processing*, vol. 22, no. 05, 2023.
  - [3] R. Alagappan, A. Ganesan, Y. Patel, T. S. Pillai, A. C. Arpaci-Dusseau, and R. H. Arpaci-Dusseau, “Correlated crash vulnerabilities,” in *12th USENIX Symposium on Operating Systems Design and Implementation (OSDI 16)*. Savannah, GA, USA: USENIX Association, 2016, pp. 151–167.
  - [4] R. Banakar, S. Steinke, B.-S. Lee, M. Balakrishnan, and P. Marwedel, “Scratchpad memory: design alternative for cache on-chip memory in embedded systems,” in *Proceedings of the tenth international symposium on Hardware/software codesign*. Estes Park, Colorado, USA: ACM, 2002, pp. 73–78.
  - [5] K. Bhardwaj, K. Chakraborty, and S. Roy, “Towards graceful aging degradation in nocs through an adaptive routing algorithm,” in *Proceedings of the 49th Annual Design Automation Conference*. San Francisco, California USA: ACM, 2012, pp. 382–391.
  - [6] T. Bjerregaard and S. Mahadevan, “A survey of research and practices of network-on-chip,” *ACM Computing Surveys (CSUR)*, vol. 38, no. 1, pp. 1–es, 2006.
  - [7] J. Cai, Z. Wu, S. Peng, Y. Wei, Z. Tan, G. Shi, M. Gao, and K. Ma, “Gemini: Mapping and architecture co-exploration for large-scale dnn chiplet accelerators,” in *2024 IEEE International Symposium on High-Performance Computer Architecture (HPCA)*, IEEE. Edinburgh, United Kingdom: IEEE, 2024, pp. 156–171.
  - [8] Y.-C. Chang, C.-T. Chiu, S.-Y. Lin, and C.-K. Liu, “On the design and analysis of fault tolerant noc architecture using spare routers,” in *16th Asia and South Pacific Design Automation Conference (ASP-DAC 2011)*, IEEE. Yokohama, Japan: IEEE, 2011, pp. 431–436.
  - [9] Y.-H. Chen, J. Emer, and V. Sze, “Eyeriss: A spatial architecture for energy-efficient dataflow for convolutional neural networks,” *ACM SIGARCH computer architecture news*, vol. 44, no. 3, pp. 367–379, 2016.
  - [10] A. Clement, E. Wong, L. Alvisi, M. Dahlin, M. Marchetti *et al.*, “Making byzantine fault tolerant systems tolerate byzantine faults,” in *Proceedings of the 6th USENIX symposium on Networked systems design and implementation*, The USENIX Association. Boston, MA: USENIX Association, 2009, pp. 153–168.
  - [11] G. Cong and K. Makarychev, “Optimizing large-scale graph analysis on multithreaded, multicore platforms,” in *2012 IEEE 26th International Parallel and Distributed Processing Symposium*. Shanghai, China: IEEE, 2012, pp. 414–425.
  - [12] J. B. Dennis and D. P. Misunas, “A preliminary architecture for a basic data-flow processor,” in *Proceedings of the 2nd annual symposium on Computer architecture*. Barcelona, Spain: ACM, 1974, pp. 126–132.
  - [13] P. Dhingra, J. Doppa, and P. P. Pande, “Hetrax: Energy efficient 3d heterogeneous manycore architecture for transformer acceleration,” in *Proceedings of the 29th ACM/IEEE International Symposium on Low Power Electronics and Design*, ser. ISLPED '24. New York, NY, USA: Association for Computing Machinery, 2024, p. 1–6. [Online]. Available: <https://doi.org/10.1145/3665314.3670814>
  - [14] P. Dhingra, J. R. Doppa, and P. P. Pande, “Atleus: Accelerating transformers on the edge enabled by 3d heterogeneous manycore architectures,” *IEEE Transactions on Computer-Aided Design of Integrated Circuits and Systems*, vol. 44, no. 8, pp. 2842–2855, 2025.
  - [15] G. Dong, Y. Hua, Y. Zhang, Z. Chen, and M. Chen, “Understanding and detecting fail-slow hardware failure bugs in cloud systems,” in *Proceedings of the 2025 USENIX Conference on Usenix Annual Technical Conference*, ser. USENIX ATC '25. USA: USENIX Association, 2025.
  - [16] B. Egger, J. Lee, and H. Shin, “Scratchpad memory management for portable systems with a memory management unit,” in *Proceedings of the 6th ACM & IEEE International Conference on Embedded Software*, ser. EMSOFT '06. New York, NY, USA: Association for Computing Machinery, 2006, p. 321–330. [Online]. Available: <https://doi.org/10.1145/1176887.1176933>
  - [17] S. Eyerman, W. Heirman, K. Du Bois, J. B. Fryman, and I. Hur, “Many-core graph workload analysis,” in *SC18: International Conference for High Performance Computing, Networking, Storage and Analysis*. Texas, Dallas: IEEE, 2018, pp. 282–292.
  - [18] Y. Feng, W. Li, and K. Ma, “Ring road: A scalable polar-coordinate-based 2d network-on-chip architecture,” in *2024 57th IEEE/ACM International Symposium on Microarchitecture (MICRO)*, IEEE. Austin, TX, USA: IEEE, 2024, pp. 871–884.
  - [19] Y. Feng, D. Xiang, and K. Ma, “A scalable methodology for designing efficient interconnection network of chiplets,” in *2023 IEEE International Symposium on High-Performance Computer Architecture (HPCA)*, IEEE. Montreal, QC, Canada: IEEE, 2023, pp. 1059–1071.
  - [20] Y. Gan, M. Liang, S. Dev, D. Lo, and C. Delimitrou, “Sage: practical and scalable ml-driven performance debugging in microservices,” in *Proceedings of the 26th ACM International Conference on Architectural Support for Programming Languages and Operating Systems*, ser. ASPLOS '21. New York, NY, USA: Association for Computing Machinery, 2021, p. 135–151. [Online]. Available: <https://doi.org/10.1145/3445814.3446700>
  - [21] Y. Gan, G. Liu, X. Zhang, Q. Zhou, J. Wu, and J. Jiang, “Sleuth: A trace-based root cause analysis system for large-scale microservices with graph neural networks,” in *Proceedings of the 28th ACM International Conference on Architectural Support for Programming Languages and Operating Systems, Volume 4*, ser. ASPLOS '23. New York, NY, USA: Association for Computing Machinery, 2024, p. 324–337. [Online]. Available: <https://doi.org/10.1145/3623278.3624758>
  - [22] P. Gratz, C. Kim, R. McDonald, S. W. Keckler, and D. Burger, “Implementation and evaluation of on-chip network architectures,” in *2006 International Conference on Computer Design*, IEEE. San Jose, CA, USA: IEEE, 2006, pp. 477–484.
  - [23] H. S. Gunawi, R. O. Suminto, R. Sears, C. Gollhofer, S. Sundararaman, X. Lin, T. Emami, W. Sheng, N. Bidokhti, C. McCaffrey *et al.*, “Fail-slow at scale: Evidence of hardware performance faults in large production systems,” *ACM Transactions on Storage (TOS)*, vol. 14, no. 3, pp. 1–26, 2018.
  - [24] M.-H. Haghbayan, A. Miele, Z. Zou, H. Tenhunen, and J. Plosila, “Thermal-cycling-aware dynamic reliability management in many-core system-on-chip,” in *2020 Design, Automation & Test in Europe Conference & Exhibition (DATE)*, IEEE. Grenoble, France: IEEE, 2020, pp. 1229–1234.
  - [25] E. Hanson, S. Li, G. Zhou, F. Cheng, Y. Wang, R. Bose, H. Li, and Y. Chen, “Si-kintsugi: Towards recovering golden-like performance of defective many-core spatial architectures for ai,” in *Proceedings of the 56th Annual IEEE/ACM International Symposium on Microarchitecture*. ON, Toronto, Canada: ACM, 2023, pp. 972–985.
  - [26] K. He, X. Zhang, S. Ren, and J. Sun, “Deep residual learning for image recognition,” in *2016 IEEE Conference on Computer Vision and Pattern Recognition (CVPR)*. Las Vegas, NV, USA: IEEE, 2016, pp. 770–778.
  - [27] Y. He, M. Hutton, S. Chan, R. De Gruijl, R. Govindaraju, N. Patil, and Y. Li, “Understanding and mitigating hardware failures in deep learning training systems,” in *Proceedings of the 50th Annual International Symposium on Computer Architecture*. FL, Orlando, USA: ACM, 2023, pp. 1–16.
  - [28] K. Hegde, P.-A. Tsai, S. Huang, V. Chandra, A. Parashar, and C. W. Fletcher, “Mind mappings: enabling efficient algorithm-accelerator mapping space search,” in *Proceedings of the 26th ACM International Conference on Architectural Support for Programming Languages and Operating Systems*. Virtual, USA: ACM, 2021, pp. 943–958.
  - [29] C. Hernández, F. Silla, and J. Duato, “A methodology for the characterization of process variation in noc links,” in *2010 Design, Automation & Test in Europe Conference & Exhibition (DATE 2010)*, IEEE. Dresden, Germany: IEEE, 2010, pp. 685–690.
  - [30] H. Huang, C. Chen, K. Chen, P. Chen, G. Yu, Z. He, Y. Wang, H. Zhang, and Q. Zhou, “Mint: Cost-efficient tracing with all requests collection via commonality and variability analysis,” in *Proceedings of the 30th ACM International Conference on Architectural Support for Programming Languages and Operating Systems, Volume 1*, ser. ASPLOS '25. New York, NY, USA: Association for Computing Machinery, 2025, p. 683–697. [Online]. Available: <https://doi.org/10.1145/3669940.3707287>
  - [31] Z. Huang, P. Chen, G. Yu, H. Chen, and Z. Zheng, “Sieve: Attention-based sampling of end-to-end trace data in distributed microservice systems,” in *2021 IEEE International Conference on Web Services (ICWS)*. Chicago, IL, USA: IEEE, 2021, pp. 436–446.
  - [32] Y. Inadomi, T. Patki, K. Inoue, M. Aoyagi, B. Rountree, M. Schulz, D. Lowenthal, Y. Wada, K. Fukazawa, M. Ueda *et al.*, “Analyzing and mitigating the impact of manufacturing variability in power-constrained supercomputing,” in *Proceedings of the international conference for high performance computing, networking, storage and analysis*. Texas, Austin: ACM, 2015, pp. 1–12.

- [33] Y. Jin, H. Wang, T. Yu, X. Tang, T. Hoefler, X. Liu, and J. Zhai, "Scalana: Automating scaling loss detection with graph analysis," in *SC20: International Conference for High Performance Computing, Networking, Storage and Analysis*, IEEE, Atlanta, GA, USA: IEEE, 2020, pp. 1–14.
- [34] J. Kaldor, J. Mace, M. Bejda, E. Gao, W. Kuropatwa, J. O'Neill, K. W. Ong, B. Schaller, P. Shan, B. Viscomi, V. Venkataraman, K. Veeraraghavan, and Y. J. Song, "Canopy: An end-to-end performance tracing and analysis system," in *Proceedings of the 26th Symposium on Operating Systems Principles*, ser. SOSP '17. New York, NY, USA: Association for Computing Machinery, 2017, p. 34–50. [Online]. Available: <https://doi.org/10.1145/3132747.3132749>
- [35] Y. Kundu, M. Kaur, T. Wig, K. Kumar, P. Kumari, V. Puri, and M. Arora, "A comparison of the cerebras wafer-scale integration technology with nvidia gpu-based systems for artificial intelligence," 2025. [Online]. Available: <https://arxiv.org/abs/2503.11698>
- [36] H. Kwon, P. Chatarasi, V. Sarkar, T. Krishna, M. Pellauer, and A. Parashar, "Maestro: A data-centric approach to understand reuse, performance, and hardware cost of dnn mappings," *IEEE Micro*, vol. 40, no. 3, pp. 20–29, 2020.
- [37] P. Las-Casas, J. Mace, D. Guedes, and R. Fonseca, "Weighted sampling of execution traces: Capturing more needles and less hay," in *Proceedings of the ACM Symposium on Cloud Computing*, ser. SoCC '18. New York, NY, USA: Association for Computing Machinery, 2018, p. 326–332. [Online]. Available: <https://doi.org/10.1145/3267809.3267841>
- [38] P. Las-Casas, G. Papakerashvili, V. Anand, and J. Mace, "Sifter: Scalable sampling for distributed traces, without feature engineering," in *Proceedings of the ACM Symposium on Cloud Computing*, ser. SoCC '19. New York, NY, USA: Association for Computing Machinery, 2019, p. 312–324. [Online]. Available: <https://doi.org/10.1145/3357223.3362736>
- [39] W. Li and P. Patras, "Stable-sketch: A versatile sketch for accurate, fast, web-scale data stream processing," in *Proceedings of the ACM Web Conference 2024*, ser. WWW '24. New York, NY, USA: Association for Computing Machinery, 2024, p. 4227–4238. [Online]. Available: <https://doi.org/10.1145/3589334.3645581>
- [40] J. Lin, P. Chen, and Z. Zheng, "Microscope: Pinpoint performance issues with causal graphs in micro-service environments," in *Service-Oriented Computing: 16th International Conference, ICSOC 2018, Hangzhou, China, November 12-15, 2018, Proceedings*. Berlin, Heidelberg: Springer-Verlag, 2018, p. 3–20. [Online]. Available: [https://doi.org/10.1007/978-3-030-03596-9\\_1](https://doi.org/10.1007/978-3-030-03596-9_1)
- [41] J. Lin, Z. Jiang, Z. Song, S. Zhao, M. Yu, Z. Wang, C. Wang, Z. Shi, X. Shi, W. Jia *et al.*, "Understanding stragglers in large model training using what-if analysis," *arXiv preprint arXiv:2505.05713*, 2025.
- [42] S.-Y. Lin and J.-Y. Lin, "Thermal-and performance-aware address mapping for the multi-channel three-dimensional dram systems," *IEEE Access*, vol. 5, pp. 5566–5577, 2017.
- [43] J. Liu, J. Zhu, S. He, P. He, Z. Zheng, and M. R. Lyu, "Logzip: extracting hidden structures via iterative clustering for log compression," in *Proceedings of the 34th IEEE/ACM International Conference on Automated Software Engineering*, ser. ASE '19. IEEE Press, 2020, p. 863–873. [Online]. Available: <https://doi.org/10.1109/ASE.2019.00085>
- [44] H. Ltaief, Y. Hong, L. Wilson, M. Jacquelin, M. Ravasi, and D. E. Keyes, "Scaling the "memory wall" for multi-dimensional seismic processing with algebraic compression on cerebras cs-2 systems," in *Proceedings of the International Conference for High Performance Computing, Networking, Storage and Analysis*, ser. SC '23. New York, NY, USA: Association for Computing Machinery, 2023. [Online]. Available: <https://doi.org/10.1145/3581784.3627042>
- [45] R. Lu, Y. Lu, Y. Jiang, G. Xue, and P. Huang, "One-size-fits-none: understanding and enhancing slow-fault tolerance in modern distributed systems," in *Proceedings of the 22nd USENIX Symposium on Networked Systems Design and Implementation*, ser. NSDI '25. USA: USENIX Association, 2025.
- [46] R. Lu, E. Xu, Y. Zhang, F. Zhu, Z. Zhu, M. Wang, Z. Zhu, G. Xue, J. Shu, M. Li, and J. Wu, "Perseus: a fail-slow detection framework for cloud storage systems," in *Proceedings of the 21st USENIX Conference on File and Storage Technologies*, ser. FAST'23. USA: USENIX Association, 2023.
- [47] R. Lu, E. Xu, Y. Zhang, Z. Zhu, M. Wang, Z. Zhu, G. Xue, M. Li, and J. Wu, "{NVMe}{SSD} failures in the field: the {Fail-Stop} and the {Fail-Slow}," in *2022 USENIX Annual Technical Conference (USENIX ATC 22)*. Carlsbad, CA, USA: USENIX Association, 2022, pp. 1005–1020.
- [48] J. Mace, R. Roelke, and R. Fonseca, "Pivot tracing: dynamic causal monitoring for distributed systems," in *Proceedings of the 25th Symposium on Operating Systems Principles*, ser. SOSP '15. New York, NY, USA: Association for Computing Machinery, 2015, p. 378–393. [Online]. Available: <https://doi.org/10.1145/2815400.2815415>
- [49] A. Marathe, Y. Zhang, G. Blanks, N. Kumbhare, G. Abdulla, and B. Rountree, "An empirical survey of performance and energy efficiency variation on intel processors," in *Proceedings of the 5th International Workshop on Energy Efficient Supercomputing*. CO, Denver, USA: ACM, 2017, pp. 1–8.
- [50] F. Merchant, *Architectures for Scientific Computing*. Singapore: Springer Nature Singapore, 2025, pp. 401–414. [Online]. Available: [https://doi.org/10.1007/978-981-97-9314-3\\_16](https://doi.org/10.1007/978-981-97-9314-3_16)
- [51] R. Miao, Z. Zhong, J. Guo, Z. Li, T. Yang, and B. Cui, "Burstsketch: Finding bursts in data streams," *IEEE Trans. on Knowl. and Data Eng.*, vol. 35, no. 11, p. 11126–11140, Nov. 2023. [Online]. Available: <https://doi.org/10.1109/TKDE.2022.3223686>
- [52] K. G. Müller, T. Vignaux, O. Lünsdorf, and S. Scherfke, "SimpY: Discrete event simulation for python," Team SimpY, 2002, accessed: 2023-11-13. [Online]. Available: <https://simpY.readthedocs.io/>
- [53] H. Namkung, Z. Liu, D. Kim, V. Sekar, and P. Steenkiste, "SketchLib: Enabling efficient sketch-based monitoring on programmable switches," in *19th USENIX Symposium on Networked Systems Design and Implementation (NSDI 22)*. Renton, WA: USENIX Association, Apr. 2022, pp. 743–759. [Online]. Available: <https://www.usenix.org/conference/nsdi22/presentation/namkung>
- [54] R. S. Nikhil *et al.*, "Executing a program on the mit tagged-token dataflow architecture," *IEEE Transactions on computers*, vol. 39, no. 3, pp. 300–318, 2002.
- [55] B. Panda, D. Srinivasan, H. Ke, K. Gupta, V. Khot, and H. S. Gunawi, "{IASO}: A {Fail-Slow} detection and mitigation framework for distributed storage services," in *2019 USENIX Annual Technical Conference (USENIX ATC 19)*. Renton, WA: USENIX Association, 2019, pp. 47–62.
- [56] T. S. Pillai, R. Alagappan, L. Lu, V. Chidambaram, A. C. Arpaci-Dusseau, and R. H. Arpaci-Dusseau, "Application crash consistency and performance with ccfs," *ACM Transactions on Storage (TOS)*, vol. 13, no. 3, pp. 1–29, 2017.
- [57] J. Redmon and A. Farhadi, "Yolo9000: Better, faster, stronger," in *2017 IEEE Conference on Computer Vision and Pattern Recognition (CVPR)*. Honolulu, HI, USA: IEEE, 2017, pp. 6517–6525.
- [58] K. Rodrigues, Y. Luo, and D. Yuan, "CLP: Efficient and scalable search on compressed text logs," in *15th USENIX Symposium on Operating Systems Design and Implementation (OSDI 21)*. USENIX Association, Jul. 2021, pp. 183–198. [Online]. Available: <https://www.usenix.org/conference/osdi21/presentation/rodrigues>
- [59] B. F. Romanescu, S. Ozev, and D. J. Sorin, "Quantifying the impact of process variability on microprocessor behavior," in *Workshop on Architectural Reliability*. Orlando, Florida: Citeseer, 2006.
- [60] S. K. Sastry Hari, M.-L. Li, P. Ramachandran, B. Choi, and S. V. Adve, "mswat: Low-cost hardware fault detection and diagnosis for multicore systems," in *Proceedings of the 42nd Annual IEEE/ACM International Symposium on Microarchitecture*. New York, NY, USA: IEEE, 2009, pp. 122–132.
- [61] P. Shukla, A. K. Coskun, V. F. Pavlidis, and E. Salman, "An overview of thermal challenges and opportunities for monolithic 3d ics," in *Proceedings of the 2019 Great Lakes Symposium on VLSI*. VA, Tysons Corner, USA: ACM, 2019, pp. 439–444.
- [62] B. H. Sigelman, L. A. Barroso, M. Burrows, P. Stephenson, M. Plakal, D. Beaver, S. Jaspan, and C. Shanbhag, "Dapper, a large-scale distributed systems tracing infrastructure," Google, Inc., Tech. Rep., 2010. [Online]. Available: <http://research.google.com/archive/papers/dapper-2010-1.pdf>
- [63] K. Simonyan and A. Zisserman, "Very deep convolutional networks for large-scale image recognition," 2015. [Online]. Available: <https://arxiv.org/abs/1409.1556>
- [64] G. M. Slota, S. Rajamanickam, and K. Madduri, "High-performance graph analytics on manycore processors," in *2015 IEEE International Parallel and Distributed Processing Symposium*. Hyderabad, India: IEEE, 2015, pp. 17–27.
- [65] C. Szegegy, W. Liu, Y. Jia, P. Sermanet, S. Reed, D. Anguelov, D. Erhan, V. Vanhoucke, and A. Rabinovich, "Going deeper with convolutions,"

- in *Proceedings of the IEEE conference on computer vision and pattern recognition*. Boston, MA, USA: IEEE, 2015, pp. 1–9.
- [66] E. Taheri, S. Pasricha, and M. Nikdast, “Deft: A deadlock-free and fault-tolerant routing algorithm for 2.5 d chiplet networks,” in *2022 Design, Automation & Test in Europe Conference & Exhibition (DATE)*, IEEE, Antwerp, Belgium: IEEE, 2022, pp. 1047–1052.
- [67] X. Tang, J. Zhai, X. Qian, B. He, W. Xue, and W. Chen, “vsensor: leveraging fixed-workload snippets of programs for performance variance detection,” in *Proceedings of the 23rd ACM SIGPLAN symposium on principles and practice of parallel programming*. Vienna Austria: ACM, 2018, pp. 124–136.
- [68] M. B. Taylor, W. Lee, S. Amarasinghe, and A. Agarwal, “Scalar operand networks: On-chip interconnect for ilp in partitioned architectures,” in *The Ninth International Symposium on High-Performance Computer Architecture, 2003. HPCA-9 2003. Proceedings.*, IEEE, Anaheim, CA, USA: IEEE, 2003, pp. 341–353.
- [69] M. Tian, J. Wang, Z. Zhang, W. Du, J. Pan, and T. Liu, “swsuperlu: A highly scalable sparse direct solver on sunway manycore architecture,” *J. Supercomput.*, vol. 78, no. 9, p. 11441–11463, Jun. 2022. [Online]. Available: <https://doi.org/10.1007/s11227-021-04270-w>
- [70] V. Tsoutsouras, D. Masouros, S. Xydis, and D. Soudris, “Softfrm: Self-organized fault-tolerant resource management for failure detection and recovery in noc based many-cores,” *ACM Transactions on Embedded Computing Systems (TECS)*, vol. 16, no. 5s, pp. 1–19, 2017.
- [71] H. Wang, Z. Wu, H. Jiang, Y. Huang, J. Wang, S. Kopru, and T. Xie, “Groot: an event-graph-based approach for root cause analysis in industrial settings,” in *Proceedings of the 36th IEEE/ACM International Conference on Automated Software Engineering*, ser. ASE ’21. Melbourne, Australia: IEEE Press, 2022, p. 419–429. [Online]. Available: <https://doi.org/10.1109/ASE51524.2021.9678708>
- [72] L. Wang, S. Jiang, S. Chen, J. Wang, and L. Huang, “Optimized mapping algorithm to extend lifetime of both noc and cores in many-core system,” *Integration*, vol. 67, pp. 82–94, 2019.
- [73] P. Wang, W. Yang, J. Fang, D. Dong, C. Huang, P. Zhang, T. Tang, and Z. Wang, “Optimizing direct convolutions on arm multi-cores,” in *SC23: International Conference for High Performance Computing, Networking, Storage and Analysis*. CO, Denver, USA: ACM, 2023, pp. 1–14.
- [74] X. Wang and J. F. Martínez, “Xchange: A market-based approach to scalable dynamic multi-resource allocation in multicore architectures,” in *2015 IEEE 21st International Symposium on High Performance Computer Architecture (HPCA)*. Burlingame, CA, USA: IEEE, 2015, pp. 113–125.
- [75] Y. Wang, T. Yang, R. Wang, and C. Tai, “Dynamic sketch: Efficient and adjustable heavy hitter detection for software packet processing,” in *2019 IEEE 8th International Conference on Cloud Networking (CloudNet)*. Coimbra, Portugal: IEEE, 2019, pp. 1–7.
- [76] T. Wu, W. Wang, Y. Yu, S. Yang, W. Wu, Q. Duan, G. Yang, J. Wang, L. Qu, and L. Zhang, “Falcon: Pinpointing and mitigating stragglers for large-scale hybrid-parallel training,” 2024. [Online]. Available: <https://arxiv.org/abs/2410.12588>
- [77] S. Xiao, X. Wang, M. Palesi, A. K. Singh, and T. Mak, “Acdc: An accuracy-and congestion-aware dynamic traffic control method for networks-on-chip,” in *2019 Design, Automation & Test in Europe Conference & Exhibition (DATE)*, IEEE, Florence, Italy: IEEE, 2019, pp. 630–633.
- [78] Z. Xu, D. Kong, J. Liu, J. Li, J. Hou, X. Dai, C. Li, S. Wei, Y. Hu, and S. Yin, “Wsc-llm: Efficient llm service and architecture co-exploration for wafer-scale chips,” in *Proceedings of the 52nd Annual International Symposium on Computer Architecture*, ser. ISCA ’25. New York, NY, USA: Association for Computing Machinery, 2025, p. 1–17. [Online]. Available: <https://doi.org/10.1145/3695053.3731101>
- [79] Z. Xu, Y. Zhang, and Z. Shen, “A fail-slow detection framework for hbm devices,” in *Proceedings of the 30th Asia and South Pacific Design Automation Conference*. Santa Clara, CA: USENIX Association, 2025, pp. 491–497.
- [80] L. Yin, A. Ghazizadeh, A. Louri, and H. Zheng, “Aries: Accelerating distributed training in chiplet-based systems via flexible interconnects,” in *2023 IEEE/ACM International Conference on Computer Aided Design (ICCAD)*. San Francisco, CA, USA: IEEE, 2023, pp. 1–9.
- [81] L. Zhang, Z. Xie, V. Anand, Y. Vigfusson, and J. Mace, “The benefit of hindsight: Tracing Edge-Cases in distributed systems,” in *20th USENIX Symposium on Networked Systems Design and Implementation (NSDI 23)*. Boston, MA: USENIX Association, 2023, pp. 321–339. [Online]. Available: <https://www.usenix.org/conference/nsdi23/presentation/zhang-lei>
- [82] N. Zhang, R. Lacouture, G. Sohn, P. Mure, Q. Zhang, F. Kjolstad, and K. Olukotun, “The dataflow abstract machine simulator framework,” in *Proceedings of the 51st Annual International Symposium on Computer Architecture*, ser. ISCA ’24. Buenos Aires, Argentina: IEEE Press, 2024, p. 532–547. [Online]. Available: <https://doi.org/10.1109/ISCA59077.2024.00046>
- [83] H. Zheng, K. Wang, and A. Louri, “Adapt-noc: A flexible network-on-chip design for heterogeneous manycore architectures,” in *2021 IEEE international symposium on high-performance computer architecture (HPCA)*, IEEE, Seoul, Korea (South): IEEE, 2021, pp. 723–735.
- [84] L. Zheng, Z. Li, H. Zhang, Y. Zhuang, Z. Chen, Y. Huang, Y. Wang, Y. Xu, D. Zhuo, E. P. Xing, J. E. Gonzalez, and I. Stoica, “Alpa: Automating inter- and Intra-Operator parallelism for distributed deep learning,” in *16th USENIX Symposium on Operating Systems Design and Implementation (OSDI 22)*. Carlsbad, CA: USENIX Association, Jul. 2022, pp. 559–578. [Online]. Available: <https://www.usenix.org/conference/osdi22/presentation/zheng-lianmin>
- [85] L. Zheng, J. Zhai, X. Tang, H. Wang, T. Yu, Y. Jin, S. L. Song, and W. Chen, “Vapro: Performance variance detection and diagnosis for production-run parallel applications,” in *Proceedings of the 27th ACM SIGPLAN Symposium on Principles and Practice of Parallel Programming*. Seoul, Republic of Korea: ACM, 2022, pp. 150–162.